

# Using Light for Better Programming of Ferroelectric Devices: Optoelectronic MoS<sub>2</sub>-Pb(Zr,Ti)O<sub>3</sub> Memories with Improved On–Off Ratios

Alexey Lipatov,\* Nataliia S. Vorobeva, Tao Li, Alexei Gruverman, and Alexander Sinitskii\*

Ferroelectric (FE) devices are conventionally switched by an application of an electric field. However, the recent discoveries of light–matter interactions in heterostructures based on 2D semiconductors and FE materials open new opportunities for using light as an additional tool for device programming. Recently, a purely optical switching of FE polarization in heterostructures comprising 2D MoS<sub>2</sub> and FE oxide perovskites, such as BaTiO<sub>3</sub> and Pb(Zr,Ti)O<sub>3</sub> (PZT), was demonstrated. In this work, it is investigated whether this optical switching has a practical value and can be used to improve functional characteristics of MoS<sub>2</sub>-PZT FE field-effect transistors for nonvolatile memory applications. It is demonstrated that the combined use of an electrical field and visible light improves the nonvolatile ON/OFF ratios in MoS<sub>2</sub>-PZT memories by several orders of magnitude compared to their purely electrical operation. The memories are read at zero gate voltage ( $V_G$ ) in darkness, but their ON and OFF currents, which routinely varied for different devices by over  $10^5$ , are achieved by programming at the same  $V_G = -6$  V with (ON state) and without (OFF state) light illumination, demonstrating its crucial importance. The light can likely serve as an important tool for better programming of a large variety of other semiconductor-FE devices.

## 1. Introduction

Monolayer molybdenum disulfide (MoS<sub>2</sub>) is a 2D semiconductor with intriguing electronic and optical properties.<sup>[1,2]</sup> In recent years, there has been a surge of interest in heterostructures comprising MoS<sub>2</sub> and various ferroelectric (FE) materials.<sup>[3–30]</sup> These MoS<sub>2</sub>-FE heterostructures were shown to be promising for a large variety of emerging electronic applications, such as FE field-effect transistors (FeFETs),<sup>[3–5,7–13]</sup> nonvolatile memories,<sup>[3,4,7,13]</sup> FE tunnel junctions,<sup>[14]</sup> ultrasensitive broadband photodetectors and phototransistors,<sup>[15–18]</sup> reconfigurable semiconductor junctions,<sup>[19,20]</sup> negative capacitance transistors with sub-60 mV/decade subthreshold swing values,<sup>[21–24]</sup> as well as acousto-electric<sup>[25]</sup> and synaptic devices.<sup>[27,28]</sup>

Interestingly, in addition to the purely electronic phenomena associated with the coupling between the polarization of an FE material and the electronic properties of MoS<sub>2</sub>, there have been several exciting recent discoveries of light–matter interactions in 2D-FE heterostructures.<sup>[4,26,29–31]</sup> For example, we previously showed that FeFET devices with MoS<sub>2</sub> channels on an FE lead zirconium titanate (Pb(Zr,Ti)O<sub>3</sub>, PZT) substrate could be switched not only electrically, but also optically, enabling a unique optoelectrical operation.<sup>[4]</sup> More recently, we demonstrated optically induced polarization switching in heterostructures based on BaTiO<sub>3</sub> (BTO) ultrathin films with MoS<sub>2</sub> or WSe<sub>2</sub> top electrodes.<sup>[26]</sup> This dual optoelectrical switching in MoS<sub>2</sub>-FE heterostructures is conceptually illustrated in **Figure 1**. **Figure 1a** shows a flake of MoS<sub>2</sub> on an FE BTO layer epitaxially grown on SrRuO<sub>3</sub> (SRO); in this scheme, the polarization of the BTO under the flake is directed upward. A conventional approach to switch the polarization of BTO under the MoS<sub>2</sub> flake is based on an application of a vertical electric field, which could be applied, for example, using a conductive tip of a scanning probe microscope (SPM). We investigated such switching in MoS<sub>2</sub>-FE heterostructures<sup>[14,28]</sup> and demonstrated that a sufficiently large positive voltage applied to the SPM probe relative to the conductive SRO sublayer could locally switch the polarization of BTO directly under the tip (**Figure 1b**). Therefore, by scanning the MoS<sub>2</sub> with a biased probe it is possible to

Dr. A. Lipatov, N. S. Vorobeva, Prof. A. Sinitskii  
Department of Chemistry  
University of Nebraska-Lincoln  
Lincoln, NE 68588, USA  
E-mail: alipatov@unl.edu; sinitskii@unl.edu

Prof. T. Li, Prof. A. Gruverman  
Department of Physics and Astronomy  
University of Nebraska-Lincoln  
Lincoln, NE 68588, USA

Prof. T. Li  
Centre for Spintronics and Quantum System  
State Key Laboratory for Mechanical Behavior of Materials  
School of Materials Science and Engineering  
Xi'an Jiaotong University  
Xi'an, Shaanxi 710049, P. R. China

Prof. A. Gruverman, Prof. A. Sinitskii  
Nebraska Center for Materials and Nanoscience  
University of Nebraska-Lincoln  
Lincoln, NE 68588, USA

 The ORCID identification number(s) for the author(s) of this article can be found under <https://doi.org/10.1002/aelm.202001223>.

DOI: 10.1002/aelm.202001223

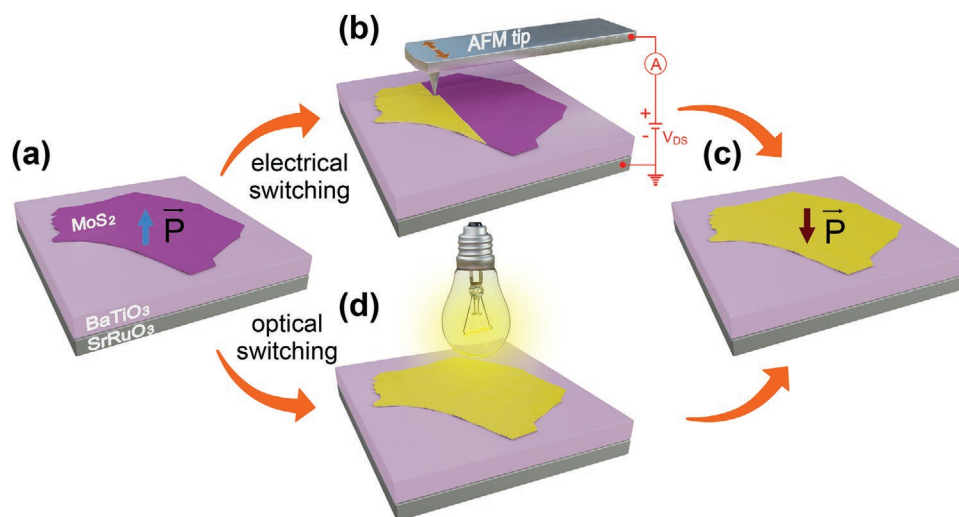


**Figure 1.** Scheme of electrical and optical switching of FE polarization of BTO under a MoS<sub>2</sub> flake in a MoS<sub>2</sub>-FE heterostructure; see text for details. The purple and yellow colors and the vertical arrows represent the polarization of BTO under the MoS<sub>2</sub> flake.

entirely switch the polarization of BTO under the flake downward,<sup>[14,28]</sup> as shown in Figure 1c. Similarly, the vertical electric field could be applied by using a global bottom gate in a FeFET configuration.<sup>[4]</sup>

A less conventional approach for the polarization switching is shown in Figure 1d. We found that the polarization of the BTO under the MoS<sub>2</sub> flake could be switched from upward to downward by visible light.<sup>[4,26]</sup> As we discussed in our previous work, this unusual possibility of a dual optoelectrical switching opens new opportunities for the MoS<sub>2</sub>-FE electronic devices, potentially simplifying the device architecture and offering additional practical functionalities, such as an instant optical erase of large data arrays.<sup>[4]</sup>

While our previous studies primarily focused on the phenomenological description and physical understanding of the light-matter interactions in MoS<sub>2</sub>-FE heterostructures,<sup>[4,26]</sup> here we demonstrate that they can be harnessed to achieve dramatically improved functional characteristics in the 2D-FE electronic devices. One particular deficiency of the MoS<sub>2</sub> FeFETs on PZT substrates reported in the previous studies is their relatively low nonvolatile ON/OFF current ratios.<sup>[4,5,13]</sup> Electronic devices based on monolayer MoS<sub>2</sub> are known to exhibit very high transistor ON/OFF current ratios (measured at different gate voltages,  $V_G$ ) of up to  $10^8$ .<sup>[2]</sup> However, for the MoS<sub>2</sub>-PZT FeFETs, the demonstrated nonvolatile memory ON/OFF ratios, though measured at the same read voltage  $V_G$  (ideally  $V_G^{\text{Read}} = 0$ ), were much more modest, on the order of  $10^3$  or less,<sup>[4,5,13]</sup> despite the demonstrated potential for an extremely wide range of possible current modulation in MoS<sub>2</sub> via electrostatic doping.<sup>[2]</sup> While in our previous studies we separately switched the FE polarization in MoS<sub>2</sub>-FE heterostructures by either electrical or optical means (Figure 1),<sup>[4,26]</sup> in this work we investigated whether by using these approaches collectively it would be possible to achieve more efficient polarization switching and demonstrate improved nonvolatile ON/OFF ratios in MoS<sub>2</sub>-PZT devices.

## 2. Results and Discussion

The experiments in this work were performed on MoS<sub>2</sub>-PZT FeFETs that are schematically shown in Figure 2a. The devices were fabricated on polycrystalline 100-nm-thick (001)-oriented tetragonal PbZr<sub>0.4</sub>Ti<sub>0.6</sub>O<sub>3</sub> films grown by metal-organic chemical vapor deposition (CVD) on a silicon wafer covered with a conductive TiO<sub>2</sub>/Ir layer; the Curie temperature of these PZT films is about 360 °C. Results of FE testing of the PZT films by Sawyer-Tower method are presented in Figure S1, Supporting Information.

For the device channels, we used triangular crystals of monolayer MoS<sub>2</sub> grown by CVD from MoO<sub>3</sub> and sulfur as described in our previous work.<sup>[32]</sup> The crystals were originally grown on Si/SiO<sub>2</sub> substrates and then transferred onto PZT substrates using a wet transfer technique.<sup>[33]</sup> Optical photograph of the MoS<sub>2</sub> crystals on Si/SiO<sub>2</sub> before the transfer is shown in Figure S2a, Supporting Information. The monolayer thickness of the MoS<sub>2</sub> crystals was confirmed by Raman spectroscopy and photoluminescence microscopy. Raman spectra of the crystals exhibited two major peaks at 382.5 cm<sup>-1</sup> ( $E_{12g}$ ) and 402.8 cm<sup>-1</sup> ( $A_{1g}$ ) (Figure S2b, Supporting Information); the spectral positions of these peaks are characteristic of monolayer MoS<sub>2</sub>.<sup>[34]</sup> Since monolayer MoS<sub>2</sub> is a direct band gap semiconductor, unlike thicker MoS<sub>2</sub> crystals that have indirect band gaps, it can be distinguished by photoluminescence microscopy.<sup>[1,32]</sup> Figure S2c, Supporting Information, shows bright emission from MoS<sub>2</sub> crystals suggesting their monolayer thickness.

After the wet transfer of the CVD-grown monolayer MoS<sub>2</sub> crystals from Si/SiO<sub>2</sub> to PZT substrates, the devices were patterned by electron beam lithography followed by electron beam evaporation of 5 nm Cr and 20 nm Au. The devices had MoS<sub>2</sub> channels bridging source (S) and drain (D) electrodes, and the conductive TiO<sub>2</sub>/Ir layer served a global gate (G) (see Figure 2a). Scanning electron microscopy (SEM) image of a representative MoS<sub>2</sub>-PZT device is shown in Figure 2b.

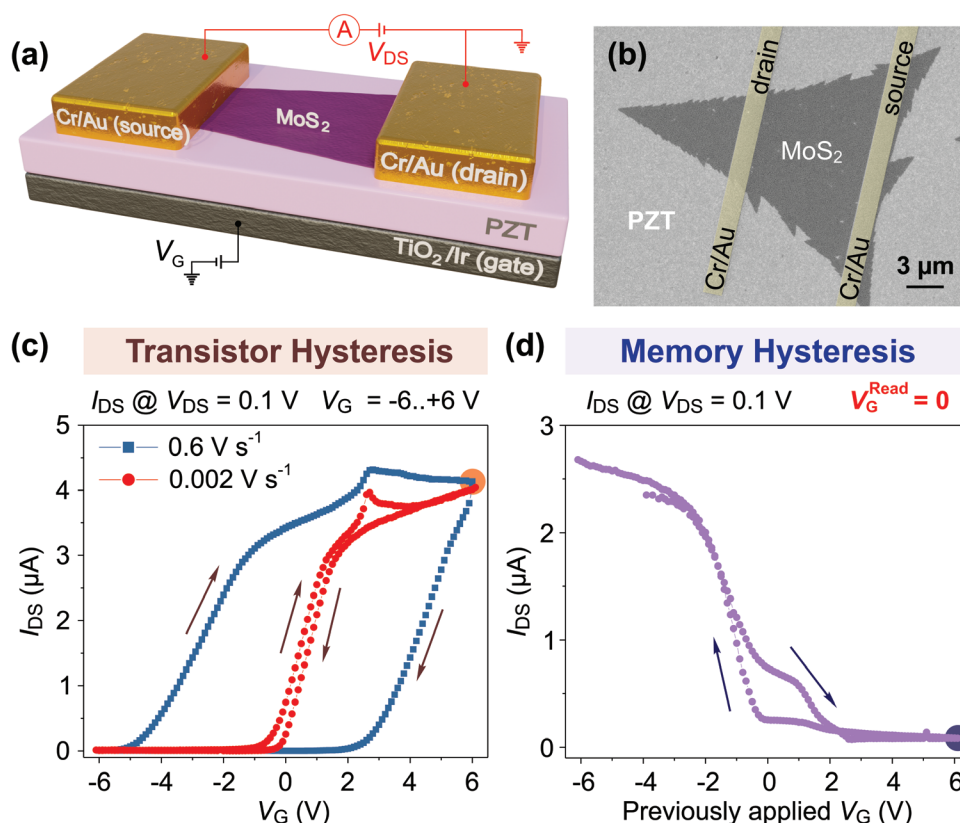


**Figure 2.** MoS<sub>2</sub>-PZT FeFET characterization. a) Scheme of MoS<sub>2</sub>-PZT FeFET. b) SEM image of a representative MoS<sub>2</sub>-PZT FeFET studied in this work. The electrodes are colored in yellow for clarity. c) Transfer characteristics of the device shown in (b) that are measured at different V<sub>G</sub> sweep rates. d) Memory hysteresis of the same device; see text for details. The curves in (c) and (d) are measured under the visible light illumination.

The electrical measurements of MoS<sub>2</sub>-PZT FeFETs were performed in vacuum at the base pressure of about  $1 \times 10^{-6}$  Torr. Prior to the measurements, the devices were evacuated for at least two days to desorb most of the atmospheric adsorbates and thus minimize their effect on the electronic transport.<sup>[35]</sup> In some electrical measurements, the devices were illuminated with a 150 W halogen light bulb with an emission spectrum covering the entire visible range, see Figure S3, Supporting Information. Figure 2c demonstrates two drain-source current ( $I_{DS}$ )-gate voltage ( $V_G$ ) dependencies for the MoS<sub>2</sub>-PZT FeFET shown in Figure 2b; the device was measured under the light illumination at the drain-source voltage ( $V_{DS}$ ) of 0.1 V. The gate voltage  $V_G$  was swept in the range from -6 V and 6 V, which exceeds the polarization switching window of this PZT substrate from -2.1 V to 2.3 V (Figure S4, Supporting Information).<sup>[4,36]</sup> We discussed in detail the transfer characteristics of similar MoS<sub>2</sub>-PZT FeFETs in our previous work.<sup>[4]</sup> We note that the width of the observed hysteresis depends on the  $V_G$  sweep rate with faster measurements resulting in wider hysteresis loops (Figure 2c). This effect, which is attributed to the interfacial charge trapping and is discussed in our previous works,<sup>[4,37]</sup> makes it necessary to indicate the  $V_G$  sweep rates for the  $I_{DS}$ - $V_G$  curves, especially when several of them are compared to each other. Figure 2c also shows that the  $I_{DS}$ - $V_G$  hysteresis loops have a clockwise direction, which does not agree with the counterclockwise polarization hysteresis of PZT.

Similar behavior was also reported for graphene-PZT devices, and the unusual hysteresis direction was generally attributed to the interfacial charge screening of FE polarization.<sup>[36–40]</sup> For the present discussion, we will refer to a single  $I_{DS}$ - $V_G$  loop in Figure 2c as transistor hysteresis, as it shows the  $I_{DS}$  while the gate voltage is actively applied.

When the gate voltage is not applied, and the device is measured under light illumination at  $V_G^{\text{Read}} = 0$ , the  $I_{DS}$  at  $V_{DS} = 0.1$  V depends on the FE polarization of PZT, which is set by the previously applied gate voltage. For example, when the device was actively gated at  $V_G = 6$  V, it showed  $I_{DS} = 4.1 \mu\text{A}$  at  $V_{DS} = 0.1$  V (see the orange circle in Figure 2c), but when the device was remeasured at  $V_G^{\text{Read}} = 0$ , it showed  $I_{DS} = 100$  nA at  $V_{DS} = 0.1$  V (see the blue circle in Figure 2d). We plotted the  $I_{DS}$  values at  $V_{DS} = 0.1$  V and  $V_G^{\text{Read}} = 0$  as a function of the previously applied gate voltage, and the resulting dependence is shown in Figure 2d. We will refer to it as memory hysteresis because it shows the range of  $I_{DS}$  currents that can be read at  $V_G^{\text{Read}} = 0$  after various write/erase gate voltages were applied to set the FE polarization of PZT to a certain state. The use of the memory hysteresis mode results in reducing the effect of charge traps on the electronic transport in MoS<sub>2</sub>-PZT devices, which visibly changes the shape of the curve in Figure 2d compared to the transistor hysteresis in Figure 2c. Figure S5, Supporting Information, provides additional information about the method to measure transistor hysteresis and memory hysteresis, which

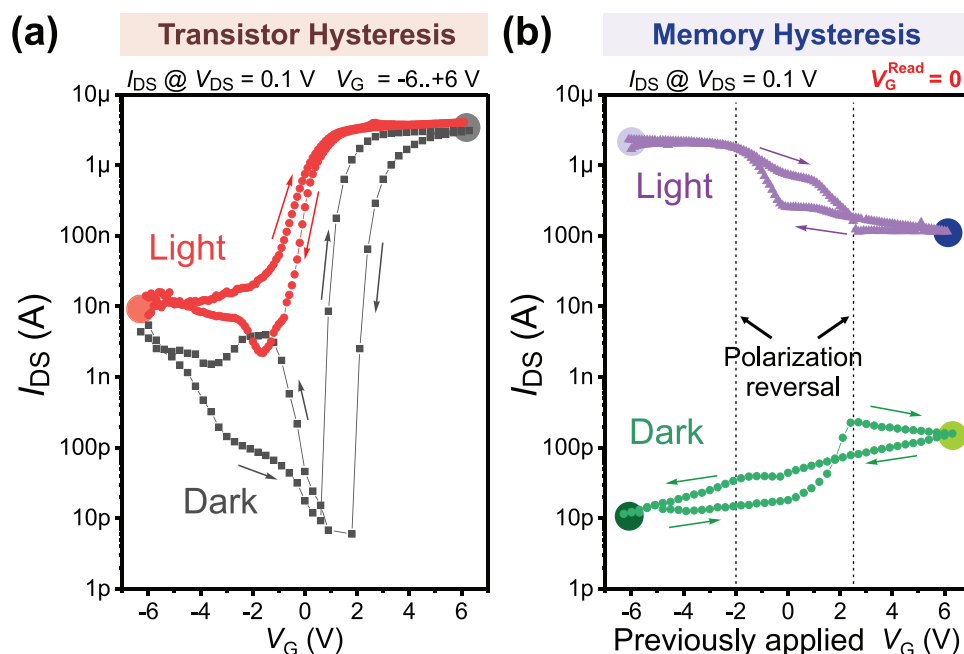


**Figure 3.** Electrical characterization of a representative MoS<sub>2</sub>-PZT FeFET in transistor and memory modes performed both in darkness and under visible light illumination. a) The  $I_{DS}$ - $V_G$  dependencies of the MoS<sub>2</sub>-PZT FeFET in the transistor mode when the bias is applied to the gate electrode. The  $V_G$  sweep rate is 0.002 V s<sup>-1</sup>. b) The  $I_{DS}$  - previously applied  $V_G$  dependencies of the MoS<sub>2</sub>-PZT FeFET in the memory mode when the measurement is performed at  $V_G^{\text{Read}} = 0$ , 30 s after application of the bias to the gate electrode. The dependencies in panels (a) and (b) were recorded both in darkness and under light illumination.

was also discussed in detail in our previous works.<sup>[4,37]</sup> Other strategies like pulse measurements, previously employed for other FE memories,<sup>[41]</sup> could also be utilized to reveal the interplay of charge trapping and FE polarization and its effect on the electronic transport in MoS<sub>2</sub>-PZT FeFETs.

The memory hysteresis in Figure 2d shows that at the read voltage of  $V_G^{\text{Read}} = 0$ , the maximum  $I_{DS}$  is observed after an application of the write voltage  $V_G = -6$  V, while the minimum  $I_{DS}$  is measured after an application of the write voltage  $V_G = 6$  V. This nonvolatile memory operation would have a modest ON/OFF current ratio of 20. However, in all measurements described so far, the switching was performed entirely by electrical means while the device was continuously exposed to visible light. On the other hand, as we outlined in the introduction and illustrated in Figure 1, light illumination could provide an additional tool for switching the FE polarization in MoS<sub>2</sub>-FE heterojunctions and might enhance the nonvolatile memory ON/OFF ratios in these devices if properly employed.

To determine the utility of visible light for improving the ON/OFF ratios in MoS<sub>2</sub>-PZT FeFETs, we first investigated how it affected the transistor and memory hysteresis loops of the same device shown in Figure 2b. The red and violet curves in **Figure 3** are the same as in Figure 2 though shown on a logarithmic  $I_{DS}$  scale. Figure 3a shows that the transfer characteristics of MoS<sub>2</sub>-PZT FeFETs measured in darkness and under illumination in the transistor mode at the same  $V_G$  sweep rate of 0.002 V s<sup>-1</sup> are qualitatively similar and exhibit the characteristic anti-hysteresis behavior.<sup>[4]</sup> Both curves show the  $I_{DS}$  of about 3 μA at  $V_G = 6$  V (see the black circle in Figure 3a) and the  $I_{DS}$  of about 5–10 nA at  $V_G = -6$  V (see the red circle in Figure 3a). The major difference between the sweeps was

observed at intermediate gate voltages, where  $I_{DS}$  is orders of magnitude higher when measured under illumination compared to  $I_{DS}$  measured in darkness. In particular, the minimum current measured in darkness is as low as  $I_{DS} = 5$  pA at  $V_G = 2$  V, while under illumination, the lowest  $I_{DS}$  of about 2.2 nA was observed at  $V_G = -1.7$  V. These measurements demonstrate the dramatic increase in electrical conductivity of MoS<sub>2</sub> under light.

However, for better understanding of the effect of visible light on the memory properties of a MoS<sub>2</sub>-PZT FeFET, it is more instructive to investigate its transfer characteristics measured in the memory mode. Figure 3b shows the memory hysteresis loops measured in darkness and under illumination, presented in semi-logarithmic scale. The memory hysteresis loops exhibit abrupt  $I_{DS}$  change in the vicinity of the PZT polarization reversal voltages, which are shown by the vertical dotted lines in Figure 3b (see also Figure S4, Supporting Information). Compared to the measurements performed in the transistor mode, the difference between the  $I_{DS}$  currents measured with and without light illumination in the memory mode is much more striking. In particular, the  $I_{DS}$  recorded at  $V_{DS} = 0.1$  V and  $V_G^{\text{Read}} = 0$  after the previously applied  $V_G = -6$  V could be as low as 11.5 pA if operated in darkness (see the dark green circle in Figure 3b) or as high as 2.3 μA if operated under illumination (see the light blue circle in Figure 3b). These curves suggest that by employing both electrical and optical stimuli it is possible to modulate the  $I_{DS}$  in MoS<sub>2</sub>-PZT FeFETs by more than five orders of magnitude. While in this case, it is possible to rationalize the increased  $I_{DS}$  under light by the photocurrent in semiconducting MoS<sub>2</sub>, in the following experiment we demonstrate that the high conductivity state (the light blue circle

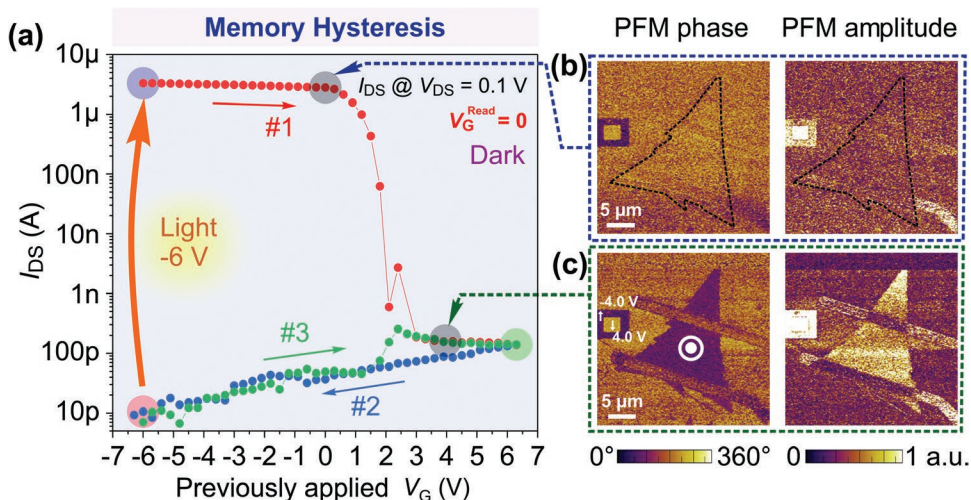


**Figure 4.** Optoelectronic memory operation of MoS<sub>2</sub>-PZT FeFET. a) The  $I_{DS}$ - $V_G$  dependence of MoS<sub>2</sub>-PZT FeFET measured in the memory mode ( $V_G^{\text{Read}} = 0$ ) in darkness. The original state shown by the blue circle is initiated by a pulse of  $V_G = -6$  V under light, while all following measurements are performed in darkness. Arrow #1 shows the direction of the first sweep from previously applied  $V_G = -6$  V to previously applied  $V_G = 6$  V, which is followed by the backward and forward sweeps (arrows #2 and #3). b,c) PFM amplitude and PFM phase images of the MoS<sub>2</sub>-PZT device in high and low conductivity states: b) after the device is illuminated (the MoS<sub>2</sub> flake is contoured for clarity) and c) after the MoS<sub>2</sub> flake is polled by a  $-4$  V pulse applied to an SPM probe. Note that a negative bias applied to the SPM probe on top of the MoS<sub>2</sub> channel corresponds to a positive bias applied to the gate electrode.

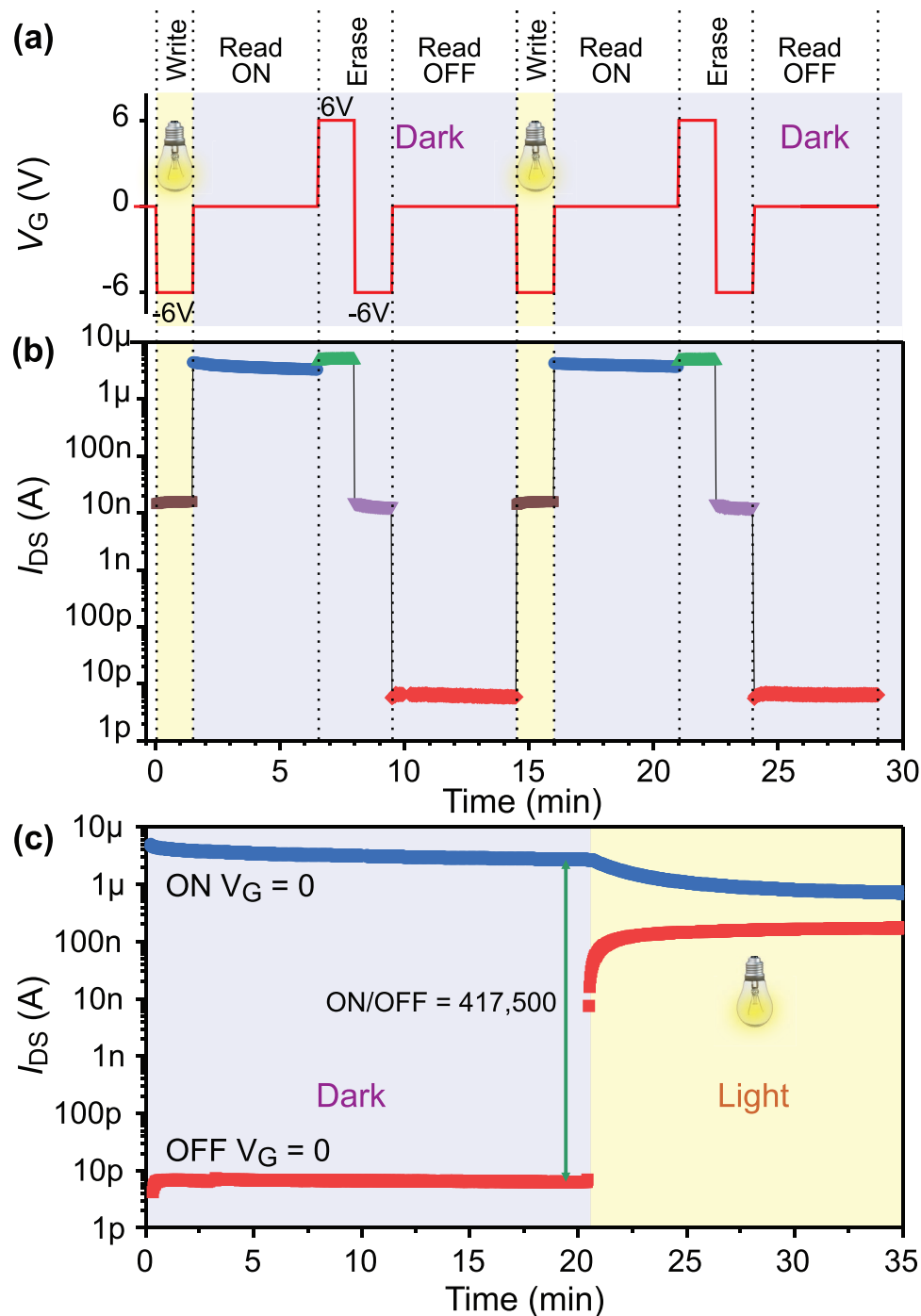
in Figure 3b) recorded under illumination retains its value in darkness. As the result, it is possible to achieve two nonvolatile  $I_{DS}$  states that could be measured under identical conditions (darkness,  $V_{DS} = 0.1$  V and  $V_G^{\text{Read}} = 0$ ) and vary by  $>10^5$ , enabling attractive nonvolatile ON/OFF ratios in the proposed optoelectrical operation mode.

Figure 4a shows an improved memory hysteresis for the same MoS<sub>2</sub>-PZT FeFET device, for which the nonvolatile ON/OFF ratio was dramatically enhanced because of the rational use of the optical and electrical stimuli. All nonvolatile  $I_{DS}$  currents shown in this memory hysteresis were measured under the same conditions: in darkness, at  $V_{DS} = 0.1$  V and  $V_G^{\text{Read}} = 0$ . The red circle in Figure 4a shows the OFF state for this device, which corresponds to the lowest nonvolatile  $I_{DS}$  current of less than 10 pA that is achieved using the previously applied  $V_G = -6$  V. Interestingly, the transition to the ON state can be accomplished at the same  $V_G = -6$  V but under the light illumination. Once this transition is completed and the device is remeasured at  $V_G^{\text{Read}} = 0$  in darkness, it shows  $I_{DS}$  of about 2  $\mu$ A (see the blue circle in Figure 4a), resulting in a nonvolatile ON/OFF ratio  $>10^5$ . It is important to emphasize that all  $I_{DS}$  values shown in Figure 4a represent the results of the measurements performed in darkness at  $V_G^{\text{Read}} = 0$ , and only the transition to the ON state requires application of  $V_G = -6$  V under illumination. In other words, the increased  $I_{DS}$  value shown by the blue circle in Figure 4a compared to the value in the red circle does not correspond to the photocurrent in semiconducting MoS<sub>2</sub> but represents the effect of light illumination on the PZT polarization (Figure 1d), as discussed in our previous works.<sup>[4,26]</sup>

The entire memory hysteresis can be followed by starting at the ON state (the blue circle). The first sweep (#1) starts with the previously applied  $V_G = -6$  V and proceeds to  $V_G = 6$  V, while the  $I_{DS}$  is recorded in the memory mode at  $V_G^{\text{Read}} = 0$  (Figure 4a). Despite being measured in darkness, the  $I_{DS}$  remains practically

the same at about 2  $\mu$ A until the previously applied  $V_G$  of about 1 V is reached, after which the  $I_{DS}$  abruptly decreases by four orders of magnitude in the vicinity of the coercive voltage of PZT ( $V_G = 2.3$  V; see Figure S4, Supporting Information). In the range of the previously applied  $V_G$  from 2.3 to 6 V, the  $I_{DS}$  remains at the same level of about 100 pA. This behavior is different from what we observed when the measurements were performed under a continuous light illumination (Figure 3b), when the conductivity varied only by about one order of magnitude over the entire sweep. The reverse sweep (#2 in Figure 4a) of the previously applied  $V_G$  from 6 V to  $-6$  V, however, resembles the sweep recorded earlier in the dark (Figure 3b): the  $I_{DS}$  slowly decreases from 100 to 10 pA, ending with the lowest conductivity state observed at the previously applied  $V_G$  of  $-6$  V (the red circle in Figure 4a). In order to complete the memory hysteresis loop with high ON/OFF ratio and return back to the high conductivity state, a single pulse of  $V_G = -6$  V under light is required. On the contrary, if the memory sweep continues in darkness from  $-6$  to 6 V, the memory hysteresis (sweep #3) would match the bottom curve in Figure 3b. If  $V_G = 6$  V is applied in the dark, the  $I_{DS}$  at  $V_G^{\text{Read}} = 0$  will be 100 pA at  $V_{DS} = 0.1$  V (see the green circle in Figure 4a).

A close inspection of the memory hysteresis in Figure 4a reveals that the high conductivity states could be achieved not only at  $-6$  V but, in general, at any negative previously applied  $V_G$  used simultaneously with the light illumination. On the other hand, if set in darkness at any previously applied  $V_G$  after another  $V_G$  pulse exceeding 2.3 V, the device will be in a low conductivity state (see low  $I_{DS}$  values for sweeps #2 and #3 in Figure 4a). The FE polarization of the device in the high and low conductivity states can be visualized by piezoresponse force microscopy (PFM), which detects its robustness (PFM amplitude) and direction (PFM phase). When the device is exposed to light at  $V_G = 0$ , the polarization ordering vanishes. The PFM imaging (Figure 4b), reveals that the FE PZT is in



**Figure 5.** Memory properties of MoS<sub>2</sub>-PZT FeFET. a) Voltage sequence for the cyclic endurance test of the MoS<sub>2</sub>-PZT FeFET. b)  $I_{DS}$  current measured at  $V_{DS} = 0.1$  V during the cyclic endurance test of the MoS<sub>2</sub>-PZT FeFET according to the scheme in (a). c) Data retention characteristics of the same device. The ON state is initiated by a pulse of  $V_G = -6$  V under light and the OFF state is initiated by a sequence of  $V_G = 6$  V and  $-6$  V pulses in darkness. The  $I_{DS}$  currents of both the ON and OFF states are recorded at  $V_G^{Read} = 0$  and  $V_{DS} = 0.1$  V as a function of time in darkness for 20 min followed by additional 15 min under illumination.

a polydomain state, characterized by low PFM amplitude and noisy PFM phase contrast.<sup>[4]</sup> Note that the polarization in the preliminary poled bare PZT film is not affected by illumination, confirming that the light interacts with MoS<sub>2</sub> flake itself, which in turn affects the FE polarization state.<sup>[4,26]</sup> These PFM images

illustrate a representative high conductivity state of the device, which is shown by the top gray circle in Figure 4a.

A representative low conductivity state of the device corresponding to the bottom gray circle in Figure 4a is illustrated by the PFM images in Figure 4c. It is achieved by an application of

a sufficiently large negative bias to an SPM tip that was put in contact with the MoS<sub>2</sub> channel of the device, which corresponds to a positive bias applied to the gate electrode. Figure 4c shows that application of -4 V bias to the tip results in FE polarization switching upward under the entire MoS<sub>2</sub> flake. This is a low conductivity state of MoS<sub>2</sub>,<sup>[14,28]</sup> which remains poorly conductive regardless of the presence or absence of light.

To demonstrate the maximum ON/OFF ratio in the MoS<sub>2</sub>-PZT device we can utilize the measurement scheme presented in Figure 5a. The experiment starts by setting the device at  $V_G = -6$  V under illumination followed by continuous measurements of the ON state in darkness at  $V_G^{\text{Read}} = 0$  for 10 min; the ON state remains very stable over this period of time (Figure 5b). After that, an application of  $V_G = 6$  V followed by  $V_G = -6$  V sets the device in the OFF state, which is also continuously measured at  $V_G^{\text{Read}} = 0$  for 10 min. This cycle is then repeated to demonstrate the consistency of the results. Figure 5b shows the  $I_{\text{DS}}$  values recorded at  $V_{\text{DS}} = 0.1$  V during the measurement scheme presented in Figure 5a.

Figure 5c shows the retention characteristics of the ON and OFF states of the MoS<sub>2</sub>-PZT device. Initiated by the writing pulse of  $V_G = -6$  V under light, the  $I_{\text{DS}}$  in the nonvolatile ON state is then measured in darkness at  $V_G^{\text{Read}} = 0$  and  $V_{\text{DS}} = 0.1$  V for 20 min. The  $I_{\text{DS}}$  value slightly decreases over time, which is likely due to the relaxation of the remaining charge traps,<sup>[37]</sup> but remains higher than 2  $\mu\text{A}$ . The OFF state is initiated by the pulse of  $V_G = 6$  V followed by the pulse of  $V_G = -6$  V, both performed in the dark. The  $I_{\text{DS}}$  in the nonvolatile OFF state is then measured for 20 min and remains stable at about  $I_{\text{DS}} = 9$  pA at  $V_{\text{DS}} = 0.1$  V (Figure 5c). The ON/OFF ratio in the optoelectrical operation mode is more than  $4 \times 10^5$ , which is four orders of magnitude larger than that reported earlier for a similar device with only electrical control.<sup>[4]</sup> It is important to note that when the light is turned on, the current in both states starts to alter (Figure 5c). Over a course of 15 min, the  $I_{\text{DS}}$  in the ON state slowly decreases from 2 to 0.9  $\mu\text{A}$ . The change of  $I_{\text{DS}}$  in the OFF state is much faster (less than 1 s) and more significant (four orders of magnitude). As we described previously, the visible light illumination has a stronger effect on the OFF state.<sup>[4]</sup>

### 3. Conclusion

In summary, we demonstrated that it is possible to employ light for effective programming of the FE devices. We investigated MoS<sub>2</sub>-PZT FeFET memory devices and showed that while their purely electrical operation produced nonvolatile ON/OFF current ratios of only about 20, a simultaneous use of the electrical and optical stimuli allows the ON/OFF ratio enhancement by four orders of magnitude up to over  $4 \times 10^5$ . Interestingly, the ON and OFF currents were achieved by device programming at the same  $V_G = -6$  V with (ON state) and without (OFF state) light illumination, demonstrating its crucial importance. The results of electrical measurements were corroborated by the PFM imaging of FE polarization of PZT in the ON and OFF states of the MoS<sub>2</sub>-PZT devices. This work suggests that light can be used as an effective tool for advanced programming of a large variety of semiconductor-FE devices allowing improved functional characteristics under electrical and optical stimuli.

### Supporting Information

Supporting Information is available from the Wiley Online Library or from the author.

### Acknowledgements

This work was supported by the National Science Foundation (NSF) through the Nebraska Materials Research Science and Engineering Center (MRSEC) (grant no. DMR-1420645). This research was performed in part in the Nebraska Nanoscale Facility: National Nanotechnology Coordinated Infrastructure, which was supported by the NSF (ECCS-1542182) and the Nebraska Research Initiative.

### Conflict of Interest

The authors declare no conflict of interest.

### Data Availability Statement

The data that support the findings of this study are available from the corresponding author upon reasonable request.

### Keywords

ferroelectric memory, field-effect transistors, lead zirconium titanate, molybdenum disulfide

Received: December 13, 2020

Revised: March 2, 2021

Published online: April 9, 2021

- [1] K. Mak, C. Lee, J. Hone, J. Shan, T. Heinz, *Phys. Rev. Lett.* **2010**, *105*, 136805.
- [2] B. Radisavljevic, A. Radenovic, J. Brivio, V. Giacometti, A. Kis, *Nat. Nanotechnol.* **2011**, *6*, 147.
- [3] H. S. Lee, S.-W. Min, M. K. Park, Y. T. Lee, P. J. Jeon, J. H. Kim, S. Ryu, S. Im, *Small* **2012**, *8*, 3111.
- [4] A. Lipatov, P. Sharma, A. Gruverman, A. Sinitiskii, *ACS Nano* **2015**, *9*, 8089.
- [5] X. W. Zhang, D. Xie, J. L. Xu, Y. L. Sun, X. Li, C. Zhang, R. X. Dai, Y. F. Zhao, X. M. Li, X. Li, H. W. Zhu, *IEEE Electron Device Lett.* **2015**, *36*, 784.
- [6] A. Nguyen, P. Sharma, T. Scott, E. Preciado, V. Klee, D. Sun, I. H. Lu, D. Barroso, S. Kim, V. Y. Shur, A. R. Akhmatkhanov, A. Gruverman, L. Bartels, P. A. Dowben, *Nano Lett.* **2015**, *15*, 3364.
- [7] C. Ko, Y. Lee, Y. Chen, J. Suh, D. Fu, A. Suslu, S. Lee, J. D. Clarkson, H. S. Choe, S. Tongay, R. Ramesh, J. Wu, *Adv. Mater.* **2016**, *28*, 2923.
- [8] Y. Liu, J. Guo, A. Yu, Y. Zhang, J. Kou, K. Zhang, R. Wen, Y. Zhang, J. Zhai, Z. L. Wang, *Adv. Mater.* **2018**, *30*, 1704524.
- [9] M. Si, P.-Y. Liao, G. Qiu, Y. Duan, P. D. Ye, *ACS Nano* **2018**, *12*, 6700.
- [10] W. C. Yap, H. J. Jiang, J. Liu, Q. Xia, W. Zhu, *Appl. Phys. Lett.* **2017**, *111*, 013103.
- [11] T. Kobayashi, N. Hori, T. Nakajima, T. Kawae, *Appl. Phys. Lett.* **2016**, *108*, 132903.
- [12] Z. Lu, C. Serrao, A. I. Khan, J. D. Clarkson, J. C. Wong, R. Ramesh, S. Salahuddin, *Appl. Phys. Lett.* **2018**, *112*, 043107.

- [13] H. W. Shin, J. Y. Son, *Electron. Mater. Lett.* **2018**, *14*, 59.
- [14] T. Li, P. Sharma, A. Lipatov, H. Lee, J.-W. Lee, M. Y. Zhuravlev, T. R. Paudel, Y. A. Genenko, C.-B. Eom, E. Y. Tsybal, A. Sinitskii, A. Gruverman, *Nano Lett.* **2017**, *17*, 922.
- [15] X. Wang, P. Wang, J. Wang, W. Hu, X. Zhou, N. Guo, H. Huang, S. Sun, H. Shen, T. Lin, M. Tang, L. Liao, A. Jiang, J. Sun, X. Meng, X. Chen, W. Lu, J. Chu, *Adv. Mater.* **2015**, *27*, 6575.
- [16] H. Fang, Z. Lin, X. Wang, C.-Y. Tang, Y. Chen, F. Zhang, Y. Chai, Q. Li, Q. Yan, H. L. W. Chan, J.-Y. Dai, *Opt. Express* **2015**, *23*, 31908.
- [17] Y. Chen, X. Wang, P. Wang, H. Huang, G. Wu, B. Tian, Z. Hong, Y. Wang, S. Sun, H. Shen, J. Wang, W. Hu, J. Sun, X. Meng, J. Chu, *ACS Appl. Mater. Interfaces* **2016**, *8*, 32083.
- [18] X. Wang, H. Shen, Y. Chen, G. Wu, P. Wang, H. Xia, T. Lin, P. Zhou, W. Hu, X. Meng, J. Chu, J. Wang, *Adv. Sci.* **2019**, *6*, 1901050.
- [19] Z. Xiao, J. Song, D. K. Ferry, S. Ducharme, X. Hong, *Phys. Rev. Lett.* **2017**, *118*, 236801.
- [20] L. Lv, F. Zhuge, F. Xie, X. Xiong, Q. Zhang, N. Zhang, Y. Huang, T. Zhai, *Nat. Commun.* **2019**, *10*, 3331.
- [21] F. A. McGuire, Y.-C. Lin, K. Price, G. B. Rayner, S. Khandelwal, S. Salahuddin, A. D. Franklin, *Nano Lett.* **2017**, *17*, 4801.
- [22] M. Si, C.-J. Su, C. Jiang, N. J. Conrad, H. Zhou, K. D. Maize, G. Qiu, C.-T. Wu, A. Shakouri, M. A. Alam, P. D. Ye, *Nat. Nanotechnol.* **2018**, *13*, 24.
- [23] X. Liu, R. Liang, G. Gao, C. Pan, C. Jiang, Q. Xu, J. Luo, X. Zou, Z. Yang, L. Liao, Z. L. Wang, *Adv. Mater.* **2018**, *30*, 1800932.
- [24] A. Nourbakhsh, A. Zubair, S. Joglekar, M. Dresselhaus, T. Palacios, *Nanoscale* **2017**, *9*, 6122.
- [25] E. Preciado, F. J. R. Schülein, A. E. Nguyen, D. Barroso, M. Isarraraz, G. Von Son, I. H. Lu, W. Michailow, B. Möller, V. Klee, J. Mann, A. Wixforth, L. Bartels, H. J. Krenner, *Nat. Commun.* **2015**, *6*, 8593.
- [26] T. Li, A. Lipatov, H. Lu, H. Lee, J.-W. Lee, E. Torun, L. Wirtz, C.-B. Eom, J. Íñiguez, A. Sinitskii, A. Gruverman, *Nat. Commun.* **2018**, *9*, 3344.
- [27] B. Tian, L. Liu, M. Yan, J. Wang, Q. Zhao, N. Zhong, P. Xiang, L. Sun, H. Peng, H. Shen, T. Lin, B. Dkhil, X. Meng, J. Chu, X. Tang, C. Duan, *Adv. Electron. Mater.* **2019**, *5*, 1800600.
- [28] A. Lipatov, T. Li, N. S. Vorobeva, A. Sinitskii, A. Gruverman, *Nano Lett.* **2019**, *19*, 3194.
- [29] D. Li, X. Huang, Z. Xiao, H. Chen, L. Zhang, Y. Hao, J. Song, D.-F. Shao, E. Y. Tsybal, Y. Lu, X. Hong, *Nat. Commun.* **2020**, *11*, 1422.
- [30] H.-J. Jin, J. Kim, Y. Kim, S. Yoon, Y. Lee, K. Kim, W. Jo, *J. Mater. Chem. C* **2020**, *8*, 3724.
- [31] K. Zhang, D. Meng, F. Bai, J. Zhai, Z. L. Wang, *Adv. Funct. Mater.* **2020**, *30*, 2002945.
- [32] A. Zobel, A. Boson, P. M. Wilson, D. S. Muratov, D. V. Kuznetsov, A. Sinitskii, *J. Mater. Chem. C* **2016**, *4*, 11081.
- [33] H. Lu, A. Lipatov, S. Ryu, D. J. Kim, H. Lee, M. Y. Zhuravlev, C. B. Eom, E. Y. Tsybal, A. Sinitskii, A. Gruverman, *Nat. Commun.* **2014**, *5*, 5518.
- [34] H. Li, Q. Zhang, C. C. R. Yap, B. K. Tay, T. H. T. Edwin, A. Olivier, D. Baillargeat, *Adv. Funct. Mater.* **2012**, *22*, 1385.
- [35] A. Sinitskii, A. Dimiev, D. V. Kosynkin, J. M. Tour, *ACS Nano* **2010**, *4*, 5405.
- [36] C. Baeumer, S. P. Rogers, R. J. Xu, L. W. Martin, M. Shim, *Nano Lett.* **2013**, *13*, 1693.
- [37] A. Lipatov, A. Fursina, T. H. Vo, P. Sharma, A. Gruverman, A. Sinitskii, *Adv. Electron. Mater.* **2017**, *3*, 1700020.
- [38] X. Hong, J. Hoffman, A. Posadas, K. Zou, C. H. Ahn, J. Zhu, *Appl. Phys. Lett.* **2010**, *97*, 033114.
- [39] E. B. Song, B. Lian, S. M. Kim, S. Lee, T. K. Chung, M. S. Wang, C. F. Zeng, G. Y. Xu, K. Wong, Y. Zhou, H. I. Rasool, D. H. Seo, H. J. Chung, J. Heo, S. Seo, K. L. Wang, *Appl. Phys. Lett.* **2011**, *99*, 042109.
- [40] W. Lee, O. Kahya, C. T. Toh, B. Özyilmaz, J.-H. Ahn, *Nanotechnology* **2013**, *24*, 475202.
- [41] E. Yurchuk, J. Muller, S. Muller, J. Paul, M. Pesic, R. Van Bentum, U. Schroeder, T. Mikolajick, *IEEE Trans. Electron Devices* **2016**, *63*, 3501.